Article:
Reimerdes, H, Duval, B. P., Harrison, J. R. et al. (16 more authors) (2017) TCV experiments towards the development of a plasma exhaust solution. Nuclear Fusion. 126007. ISSN: 1741-4326

https://doi.org/10.1088/1741-4326/aa82c2

TCV Experiments towards the Development of a Plasma Exhaust Solution

H. Reimerdes[1], B.P. Duval[1], J.R. Harrison[2], B. Labit[1], B. Lipschultz[3], T. Lunt[4], C. Theiler[1], C.K. Tsui[1,5], K. Verhaegh[1,3], W.A.J. Vijvers[6], J.A. Boedo[5], G. Calabro[7], F. Crisanti[7], P. Innocente[8], R. Maurizio[1], V. Pericoli[8], U. Sheikh[1], M. Spolare[8], N. Vianello[1,8], the TCV team[a] and the EUROfusion MST1 team[b]

[1]*Ecole Polytechnique Fédérale de Lausanne (EPFL), Swiss Plasma Center (SPC), 1015 Lausanne, Switzerland*

[2]*CCFE, Culham Science Centre, Abingdon, Oxon, OX14 3DB, United Kingdom*

[3]*York Plasma Institute, University of York, Heslington, York, YO10 5DD, United Kingdom*

[4]*Max-Planck Institute for Plasma Physics, Boltzmannstr. 2, 85748 Garching, Germany*

[5]*University of California – San Diego (UCSD), La Jolla, CA 92093, USA*

[6]*DIFFER - Dutch Institute for Fundamental Energy Research, De Zaale 20, 5612 AJ Eindhoven, Netherlands*

[7]*ENEA, C.R. Frascati, Via E. Fermi 45, 00044 Frascati, Italy*

[8]*Consorzio RFX, Corso Stati Uniti 4, 35127 Padova, Italy*

E-mail contact of main author: holger.reimerdes@epfl.ch

Abstract. Research towards a plasma exhaust solution for a fusion power plant aims at validating edge physics models, strengthening predictive capabilities and improving the divertor configuration. The TCV tokamak is extensively used to investigate the extent that geometric configuration modifications can affect plasma exhaust performance. Recent TCV experiments continue previous detachment studies of Ohmically heated L-mode plasmas in standard single-null configurations, benefitting from a range of improved diagnostic capabilities. Studies were extended to nitrogen seeding and an entire suite of alternative magnetic configurations, including flux flaring towards the target (X divertor), increasing the outer target radius (Super-X) and movement of a secondary x-point inside the vessel (X-point target) as well as the entire range of snowflake configurations. Nitrogen seeding into a snowflake minus configuration demonstrated a regime with strong radiation in the large region between the two x-points, confirming EMC3-Eirene simulations, and opening a promising path towards highly radiating regimes with limited adverse effects on core performance.

1. Introduction

A plasma exhaust solution for a fusion power plant must ensure acceptable conditions at the walls while maintaining sufficient core performance. Fusion power plants based on the tokamak concept will therefore likely require the expulsion of a high fraction of the plasma heating power as radiation and the establishment of a pressure gradient along the scrape-off layer (SOL) field lines, characteristic of operation in a detached divertor regime [1]. Since it is uncertain whether such operation in the elementary single null divertor can meet all requirements of a power plant, present research aims at validating physics models to strengthen predictive capabilities and at improving the operating regime and the magnetic configuration [2]. The TCV tokamak is used to investigate the extent to which geometric modifications of the magnetic

[a]See the author list of "S. Coda et al., Nucl. Fusion **57** (2017) 102011".

[b]See the author list of "H. Meyer et al., Nucl. Fusion **57** (2017) 102014".

configuration can affect the plasma exhaust performance, focusing, in particular, on the access to a detached operating regime.

Detachment is obtained when the plasma temperature in front of the target is sufficiently low that neutral friction can sustain a gradient in the plasma pressure along the magnetic field lines in the divertor [3]. The fundamental dependencies are described by the 2-point model [4], which relates the plasma temperature T and density n at the divertor targets ('t') to the conditions in the vicinity of the closed field lines usually referred to as upstream ('u'). In its extended form, the 2-point model relates the plasma temperature at the target T_t to the upstream density n_u, the parallel heat flux as well as geometric parameters such as connection length $L_\parallel$ and target radius R_t [5,6],

$$T_\mathrm{t} \propto \frac{q_{\parallel,\mathrm{u}}^{10/7}(1-f_\mathrm{rad})^2}{n_\mathrm{u}^2 L_\parallel^{4/7}} \frac{R_\mathrm{u}^2}{R_\mathrm{t}^2} \ . \tag{1}$$

The upstream parallel heat flux, which is here evaluated at the separatrix,

$$q_{\parallel,\mathrm{u}} = \frac{B_\mathrm{tot,u}}{B_{p,\mathrm{u}}} \frac{c_\mathrm{div} P_\mathrm{sep}}{2\pi R_\mathrm{u} \lambda_\mathrm{q,u}} \ , \tag{2}$$

depends on the power crossing the separatrix, P_sep, the fraction of this power that is directed towards the investigated divertor target, c_div, and the characteristic width of the SOL heat flux, $\lambda_\mathrm{q,u}$. While increasing the plasma density and thereby n_u is an efficient means to lower T_t, its maximum value is limited by core confinement degradation and ultimately the plasma stability. Therefore, other means to lower T_t must be found. A commonly used technique to lower the temperature is impurity seeding, which increases the radiation fraction in the divertor, $f_\mathrm{rad} = P_\mathrm{rad}^\mathrm{div}/P_\mathrm{sep}$. Novel magnetic configurations seek to facilitate the decrease of T_t and thereby access to detachment by increasing the achievable f_rad, increasing $L_\parallel$, increasing R_t, increasing $\lambda_\mathrm{q,u}$ or by a combination of several of these aspects.

Recent TCV experiments continue previous detachment studies in conventional single null [7] and snowflake configurations [8]. They use the unique shaping capabilities of TCV and benefit from diagnostic enhancements, described in section 2. Detachment in Ohmically heated plasmas is characterised with unprecedented detail in section 3. These studies include variations of flux expansion and divertor leg length. The detachment studies are then extended to an entire set of proposed alternative configurations, including the X divertor [9], Super-X divertor [10], snowflake divertor [11] and X-point target divertor [12] in section 4. A summary is presented in section 5.

2. The TCV tokamak as a facility to investigate plasma exhaust

TCV is a medium size tokamak (major radius $R_0 = 0.88$ m, aspect ratio $A = 3.6$) with a toroidal field $B_0 \leq 1.45$ T. TCV has a highly-elongated vessel and 16 independently powered poloidal field coils providing unique shaping capabilities that can generate a wide variety of divertor configurations. The near-complete coverage of TCV surfaces with graphite tiles imposes few constraints on the placement of power and particle loads and TCV is extensively used to study divertor physics and alternative divertor concepts. Fuelling and impurity seeding is carried out using valves on the floor.

Recent SOL transport and detachment experiments have benefited from a range of improved diagnostic capabilities.

- A new 32-chord divertor spectroscopy system (DSS), designed to diagnose a wide range of divertor configurations, and track the characteristics and extent of the detachment

region [13]. The Stark broadening of the $n = 6,7$ Balmer series lines yields an estimate of the electron density. In addition, a new method has been developed to utilise Balmer line ratios to separate the recombination and excitation contributions to the emission of individual lines, and use the recombination contribution to estimate the recombination rate R_L [13].

- The infrared thermography diagnostic has been upgraded with an additional view of the lower inner wall and the addition of a second fast-framing MWIR camera for simultaneous heat flux measurements at the inner and outer divertor targets of a wide range of diverted configurations [14].
- The wall-mounted Langmuir probe array on the inner wall was extended to lower positions. A subset of probes now uses roof-top tips for more reliable measurements when the grazing angle of the incident magnetic field lines is small [6].
- A fast reciprocating probe, previously mounted on NSTX [15], was installed on an outboard mid-lane port and yields SOL temperature and density measurements.
- Baratron pressure gauges, on the floor and outboard mid-plane, provide absolutely calibrated neutral pressure measurements [6].

3. Detachment in TCV

Recent TCV detachment experiments were conducted in L-mode plasmas in the standard TCV lower single-null (SN) divertor configuration, characterised by a short inner and longer outer divertor leg, FIG. 1(a). The angle of the SOL flux surfaces with respect to the divertor targets is usually ~90 degrees. For these experiments the toroidal field is directed in the 'reverse' direction, i.e. corresponding to an ion ∇B drift direction away from the x-point, similar to previous studies [7]. This choice increases the L-H power threshold permitting L-mode experiments at high plasma current and heating power.

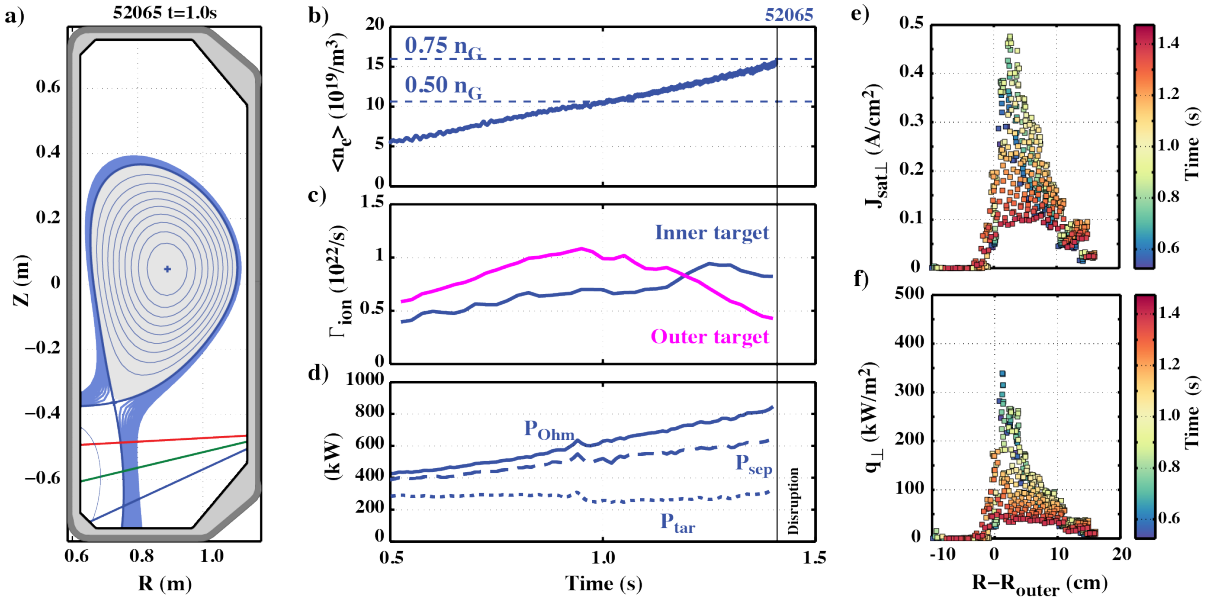

FIG. 1. (a) Standard TCV divertor configuration ($B_T = 1.42$ T, $I_P = 340$ kA, $q_{95} = 2.5$) and evolution of (b) the line averaged density $\langle n_e \rangle$, (c) total ion fluxes Γ_{ion} to the inner and outer targets and (d) Ohmic heating power P_{Ohm}, power crossing the separatrix $P_{sep} \approx P_{Ohm} - P_{rad,core}$ and power at the wall $P_{tar} \approx P_{Ohm} - P_{rad}$ in an Ohmically heated density ramp experiment. Also shown are the (e) ion current $j_{sat,\perp}$ and (f) heat flux profiles $q_\perp$ measured with Langmuir probes at the outer target.

3.1. Density ramp experiments

The detachment behaviour is probed in density ramp experiments, where the electron density is measured along a central interferometer chord to yield the line averaged density $\langle n_e \rangle$, FIG. 1(b) [6,16]. Swept Langmuir probes estimate the ion current to the target, Γ_{ion}, FIG. 1(c), the electron density at the target, $n_{e,t}$, and the electron temperature at the target, $T_{e,t}$. At low density, Γ_{ion} increases with $\langle n_e \rangle$, but the increase is slower than the $\propto \langle n_e \rangle^2$ dependence predicted by the 2-point model in the high recycling regime, assuming that $n_{e,u} \propto \langle n_e \rangle$. At sufficiently high density, Γ_{ion} at the outer target ceases to increase and 'rolls over' at $t \approx 1.0$s, FIG. 1(c), when $\langle n_e \rangle \approx 1.0 \times 10^{20} m^{-3}$. This deviation from the expected dependence correlates with a pressure loss along the field line, which in this work is referred to as the onset of detachment. Systematic changes in the SOL width, with reciprocating probe measurements at the outboard mid-plane actually indicating a gradual broadening of the SOL with density [17], together with possible changes of the ratio of $\langle n_e \rangle$ and $n_{e,u}$ add some uncertainty to the determination of the detachment onset. In the reference configuration, only the ion current to the outer divertor rolls over before a disruptive density limit is encountered at ~70% of the Greenwald density. The inner divertor generally remains attached. The ion current density and heat flux at the outer target decrease most near the separatrix, FIG. 1(e,f). The profiles for the highest density values are characteristic of 'partial detachment' [18].

While increasing $\langle n_e \rangle$ increases the radiated power, which in un-seeded discharges is expected to arise mainly from the ubiquitous carbon impurities, it also increases the Ohmic heating power, P_{Ohm}, FIG. 1(d). The radiated power and its poloidal distribution is obtained through a tomographic inversion of foil bolometer measurements. The increase of the radiated power P_{rad} with $\langle n_e \rangle$ typically cancels the increase in P_{Ohm}, leaving the power that must be exhausted at the targets P_{tar} approximately constant, FIG. 1(d). Since a significant fraction of the radiation originates from outside the last closed flux surface (LCFS), the power crossing the separatrix in the plasma channel, P_{sep}, actually increases with $\langle n_e \rangle$, FIG. 1(d). At low $\langle n_e \rangle$ the radiation emissivity is highest close to both targets. As $\langle n_e \rangle$ increases, the total emissivity peak moves from the outer target towards the x-point. This movement is also seen in the line-integrated measurements along chords that intersect the outer divertor leg, FIG. 2(a). At the inner target the total emissivity increases and the emitting region extends towards and eventually past the x-point.

A tangential camera system simultaneously images the divertor at four wavelengths, including C III, D_α, D_γ and C II. Tomographic inversion yields the poloidal emissivity distribution [16]. The region of C III emissivity starts to recede from the strike point somewhat before the roll over in the ion current. The cut-off towards the target is expected for electron temperatures in the range of 3-8eV with a cross-comparison with target Langmuir probes indicating a temperature of 7-8eV [6]. This C III front moves approximately linearly with density up the divertor leg towards the x-point, FIG. 2(b). The movement is quasi-static and appears stable. At detachment onset the C III emissivity is peaked at the x-point and extends half-way down the leg. Once the C III front reaches the x-point it stops and the density can be further increased until a disruptive density limit occurs. Line integrated radiation measurements along bolometer chords, FIG. 2(a), show that the C III moves together with the high radiation region. A comparison with the evolution of the D_α distribution indicates that the ionisation region follows the C III front and the radiation region up the divertor leg.

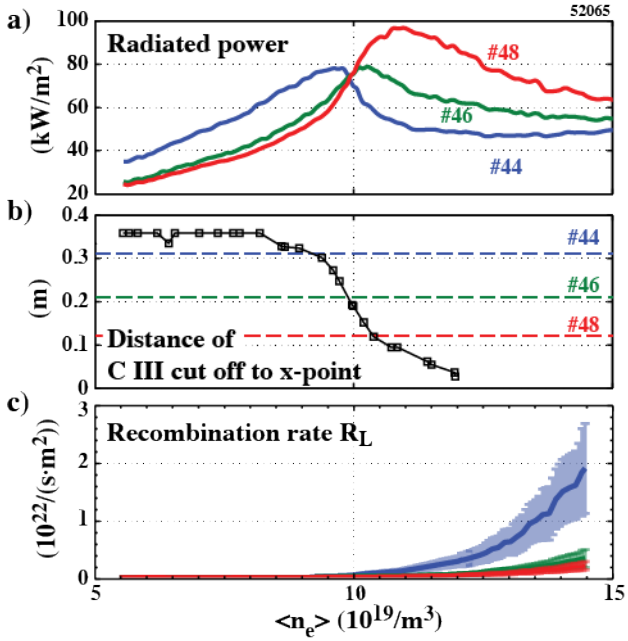

FIG. 2: Density dependence of (a) radiation emission along the chords shown in FIG. 1(a), (b) the poloidal distance of the C III cut-off from the x-point and (c) the line integrated recombination rate R_L along chords similar to the bolometer chords estimated from DSS measurements of the Balmer spectrum.

Spectroscopy indicates that recombination first increases at the target. At higher $\langle n_e \rangle$, the emission near the target develops a tail that extends towards the x-point. However, the recombination rate, inferred from DSS measurements of the Balmer spectrum, always remain highest on the chord closest to the target (similar geometry as the blue bolometer chord in FIG. 1(a), 5 cm above the target), FIG. 2(c) [13]. The density determined by Stark broadening does, in particular, not show the roll-over observed by Langmuir probes at the target. This suggests that the recombination front never moves more than a few cm above the target, which differs from observations in other, higher density tokamaks, where the recombination front moves towards the x-point. This difference may be due to a longer mean free path for ionisation, typically longer than the width of the TCV divertor leg. Neutrals are not well-confined leading to less ionisation and, potentially, a slower rise of the divertor density and, hence, a slower rise in charge exchange and recombination processes [13].

Experiments at lower plasma current (I_P = 250 kA) reach detachment onset at somewhat lower density than the described high current scenarios. The role over in Γ_{ion} is immediately followed by a disruption before a substantial reduction of Γ_{ion}, indicative of a larger pressure reduction, i.e. deeper detachment, can be obtained.

3.2 Flux expansion effect on detachment

The magnetic geometry in the divertor can be modified by changing the flux expansion at the target, $f_{x,t} \equiv dr_t/dr_u$, where dr is the distance between flux surfaces. Flaring of the flux surfaces near the target is avoided to distinguish the configuration from X divertor configurations, discussed in section 4.1. TCV experiments achieved such variations of the flux expansion ranging from $f_{x,t}$ = 2.0 to $f_{x,t}$ = 8.5. Increasing $f_{x,t}$ increases the wetted area and, hence, decreases the peak heat load on the targets. In addition to a geometric reduction of the heat flux onto the target, a greater wetted area is predicted to increase the interaction with neutrals [9]. The realised increase in $f_{x,t}$ also increases the connection length, $L_{||}$, and hence the SOL volume,

V_{SOL}, by approximately 60%[c], FIG. 3(a) (insert). The resulting increased divertor leg width may also improve the confinement of neutrals being less transparent to neutrals for the same local parameters.

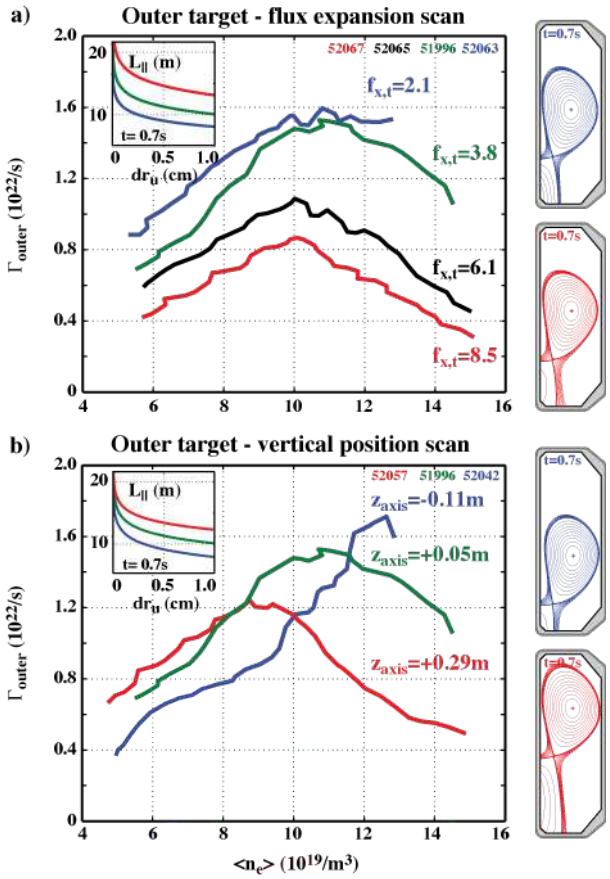

FIG. 3. Density dependence of the ion current to the outer target for (a) several flux expansions ($z_{axis} \approx 0.05$m) and (b) several vertical positions ($f_{x,t} \approx 4$). Inserts show the connection lengths.

The density required for the onset of detachment, i.e. when the total ion current to the outer target reaches a maximum, decreases only weakly with increasing $f_{x,t}$, FIG. 3(a). As the onset of detachment is expected to depend strongly on the plasma temperature at the target, the observed decrease of the density at the onset of detachment can be compared with the expectation based on the 2-point model, Eq. (1),

$$n_u(T_t = const.) \propto \frac{q_{||,u}^{5/7}(1-f_{rad})}{L_{||}^{2/7} R_t} \quad . \tag{3}$$

The increase of $L_{||}$ in the flux expansion scan by 60% alone is, therefore, expected to decrease <n_e> at the onset of detachment by approximately 15%, which is within the uncertainty of the observed dependence, FIG. 3(a). The effect of the flux expansion becomes more significant when the density is further increased, where the drop in Γ_{ion} is considerably stronger at high flux expansion, FIG. 3(a).

[c] The values of $L_{||}$ are evaluated for the flux surfaces with an outboard mid-plane distance from the LCFS of 5 mm, which corresponds to a typical power fall-off length.

3.3 Divertor leg length effect on detachment

Alternatively, connection length and divertor volume can be changed by vertically shifting the plasma. TCV experiments realised variations of the vertical axis positions, z_{axis}, from -0.11 m to +0.29 m corresponding to poloidal divertor leg lengths from 0.23 m to 0.63 m, respectively. With the flux expansion fixed at $f_{x,t} \approx 4.0$, this variation of z_{axis} led to an increase of $L_{\parallel}$ of 50%, FIG. 3(b) (insert), which is comparable to the variation of $L_{\parallel}$ in the flux expansions scan, section 3.2.

Conversely to $f_{x,t}$, the divertor leg length has a stronger effect on the onset of detachment. The increase of the divertor leg length by a factor of 2.7 leads to a decrease of the density at the roll-over of Γ_{ion} by ~30%. This decrease is significantly larger than the decreases expected according to Eq. (3) due to the increase of $L_{\parallel}$ alone. The difference in the dependence of the onset of detachment on flux expansion and divertor leg length may be explained by their effect on the power fall off length $\lambda_{q,u}$. Experiments in Ohmically heated, low density TCV plasmas with attached divertor conditions have shown that flux expansion does not affect $\lambda_{q,u}$., whereas an increase of the divertor leg length increases $\lambda_{q,u}$ [14,19]. An increase of the divertor leg length from of 0.23 m to 0.63 m may increase $\lambda_{q,u}$ by as much as 40%. Assuming that this increase in $\lambda_{q,u}$ leads to a proportional decrease of $q_{\parallel,u}$, Eq. (2), and occurs equally at higher densities, it would be sufficient to explain the entire observed decrease of $<n_e>$ at the onset of detachment by ~30%. Similar to higher flux expansion a longer leg also allows for a much deeper detachment and a higher maximum core density, FIG. 3(b).

4. Alternative configurations

As the flux expansion is limited by the grazing angle of the field line at the target and the divertor leg length by the increased cost of the required toroidal field coils, the potential of these basic geometric modifications to improve the power exhaust performance in a fusion power plant is limited. The potential of alternative configurations is therefore assessed.

4.1. The X divertor

The X-divertor concept [9] is characterised by a flaring of the flux surfaces towards the target and large values of $f_{x,t}$. The resulting large interaction area of the plasma with neutrals at the target should facilitate detachment. Flaring decreases that area towards the x-point and should diminish the movement of the detachment region up the divertor leg [9]. In contrast to the standard TCV divertor configurations investigated in section 3, the flaring of the flux surfaces at the target also leads to a 'closed' divertor geometry at the separatrix.

TCV examined divertor configurations ranging from $f_{x,t} = 2$ and concentrating flux surfaces towards the target up to $f_{x,t} = 21$ with strong flux surface flaring [6], FIG. 4. Density ramps were performed (I_p = 340 kA). Similar to the flux expansion scan (section 3.2), there is no clear indication that flaring reduces the detachment threshold density. However, once the C III emission cut-off front, which coincides with plasma temperatures at which the interaction with neutrals is expected to become important, leaves the floor, the flux flaring starts to affect the detachment behaviour with a larger $f_{x,t}$ leading to a slower movement of the C III emission cut-off front towards the x-point, FIG. 4. This effective delay is limited to the lower third of the divertor leg, which corresponds approximately to the region with a flux surface flaring towards the target. Such a behaviour is consistent with the alleged advantage of the X divertor as well as previous TCV experiments [7] and more recent DIII-D experiments [20]. It, however, remains to be seen to what extent the slower displacement of the CIII front in the highly flared divertor can be explained by a geometrical projection of the parallel dynamics into the poloidal plane.

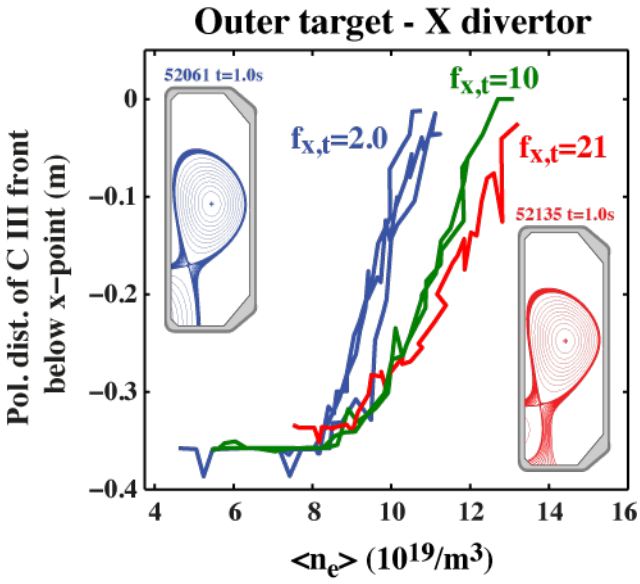

FIG. 4. Movement of the C III cut-off front in density ramps (B_T = 1.42 T, I_P = 340 kA) with different flux flaring at the outer target [6].

4.2 The Super-X divertor

The Super-X concept [10] extends the flaring to total flux expansion by increasing the target major radius R_t. The decrease in magnetic field with R introduces a gradient in $q_{||}$ along the field lines. This reduction of $q_{||,t}$ should lead to a strong increase of the target density, $n_{e,t} \propto R_t^2$ and a corresponding decrease in the target temperature, $T_{e,t} \propto R_t^{-2}$, Eq. (1), thereby lowering the detachment density threshold, Eq. (3) [21]. The decrease in $q_{||}$ towards the target is also thought to have a stabilising effect on the radiation front location and should facilitate its control. A greater distance between the radiation front and the closed flux surfaces should also reduce detrimental effects on core performance.

TCV examined divertor configurations ranging from an outer target radius, R_t^{outer} of 0.62 m to 1.06 m [6], FIG. 5. Density ramps (I_p = 340 kA) were performed. For R_t^{outer} from 0.69 m to 0.91 m Langmuir probe measurements resolve the outer target profiles and support the expected $1/R_t$ dependence of $q_{||}$. However, both the observed R_t dependence of the target density and target temperature, are weaker than expected and, contrary to expectation, the threshold density remained similar or slightly increased. Furthermore, the movement of the C III cut-off front shows no dependence on R_t, FIG. 5. Dedicated experiments [6] showed that neither differences in the fuelling location nor flux expansion explain this unexpected detachment behaviour.

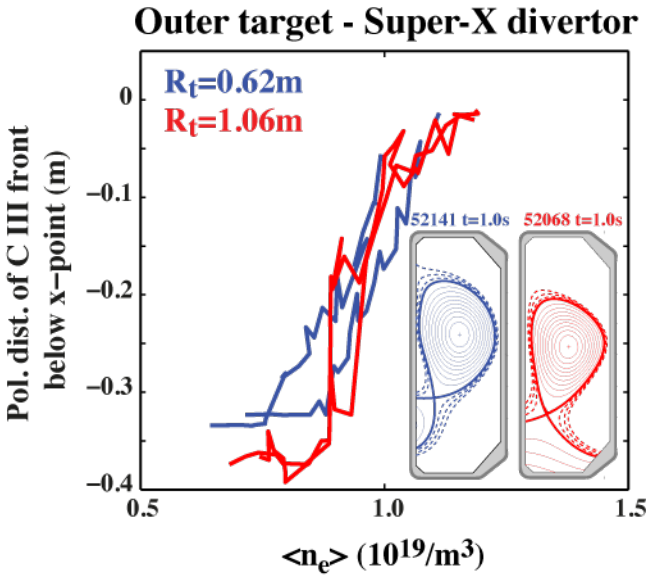

FIG. 5. Movement of the C III cut-off front in density ramps (B_T = 1.42 T, I_P = 340 kA) with different outer target radii [6].

4.3. The Snowflake divertor

The snowflake (SF) divertor [11] introduces a second order null-point. Practically, SF configurations have two nearby x-points and can be parameterised by a flux coordinate of the secondary x-point [22], such as the corresponding upstream distance to the separatrix, $dr_{u,X2}$. The snowflake plus (SF+) or minus (SF-) depend on whether the secondary x-point is located in the private or common flux region. The SF configuration increases $L_{\parallel}$ and V_{SOL} near the separatrix. The increase in V_{SOL} is thought to enhance volume power losses and thereby facilitate access to detachment. The relatively large region of low poloidal field in the vicinity of the null points may drive instabilities and enhance turbulent cross-field transport, which should widen the SOL, reducing peak heat fluxes [23]. There is, however, nothing to prevent the radiation or detachment front moving into the null-region.

TCV has examined the entire range of SF configurations, FIG. 6(a-c), albeit at a reduced plasma current (I_p = 250 kA). Contrary to the first radiative SF experiments [8], recent experiments were carried out in reversed field. In TCV's geometry, only the HFS and LFS SF-configurations can increase $L_{\parallel}$ across a significant fraction of one side of the SOL, FIG. 6(e,f). This is a consequence of the relatively large width of the TCV SOL with respect to TCV's linear dimensions and will change in a reactor-sized device, where the SF+ will increase $L_{\parallel}$ on both sides of the divertor [24]. The strike points (SP) are labelled from 1 to 4 starting at the highest strike point on the inner wall and counting counter-clockwise.

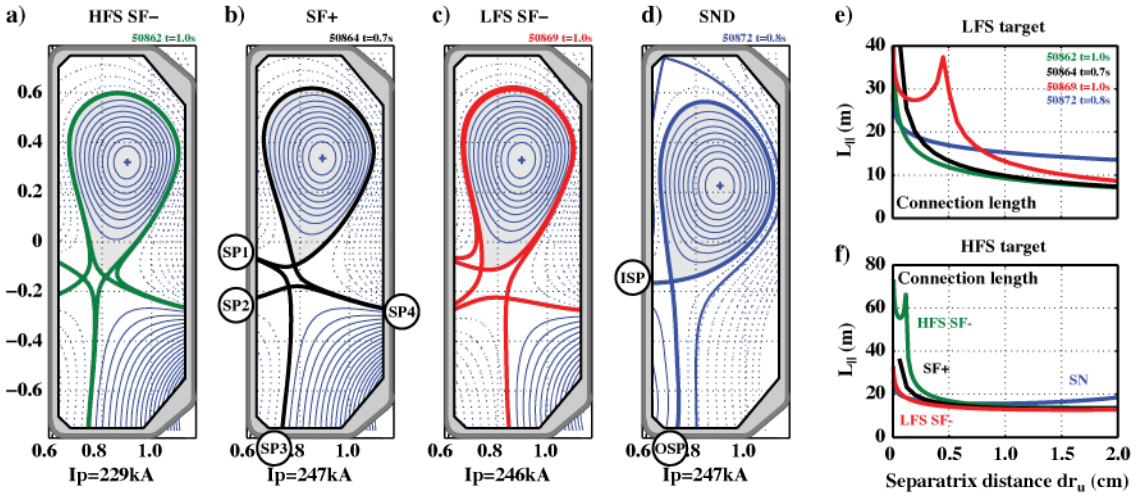

FIG.: 6. Realised SF configurations (a-c) and SN reference (d) together with the connection length from the outboard mid-plane downwards (e) and upwards (f) to the targets. Labels in (b) and (d) indicate the customary notation of strike points.

TCV has realised LFS SF- configurations with x-point separations $dr_{u,X2}$ ranging from 3 mm to 28 mm. In the high recycling regime, the particle flux to SP2 increases with increasing $dr_{u,X2}$, as a higher fraction of the SOL is directed to this strike point, FIG. 7(a). Simultaneously, the particle flux to SP4 decreases, qualitatively consistent with expectations and previous TCV findings [25], FIG. 7(b). It is, however surprising that even when $dr_{u,X2}$ exceeds the typical characteristic power fall off length of ~7 mm in these plasmas, the majority of the particles are still directed to SP4. Density ramp experiments indicate that the onset of detachment at SP2 is independent of $dr_{u,X2}$ and obtained at $\langle n_e \rangle \approx 8\text{x}10^{19}\text{m}^{-3}$, i.e. similar to SN configurations at this plasma current. The decrease of $\Gamma_{ion,SP2}$ is, however, much faster in all SF- configurations and $\langle n_e \rangle$ can be further increased up to full detachment of SP2, FIG. 7(a). The onset of detachment at SP4 occurs at similar densities, but deeper detachment is only obtained at the smallest $dr_{u,X2}$, FIG. 7(b).

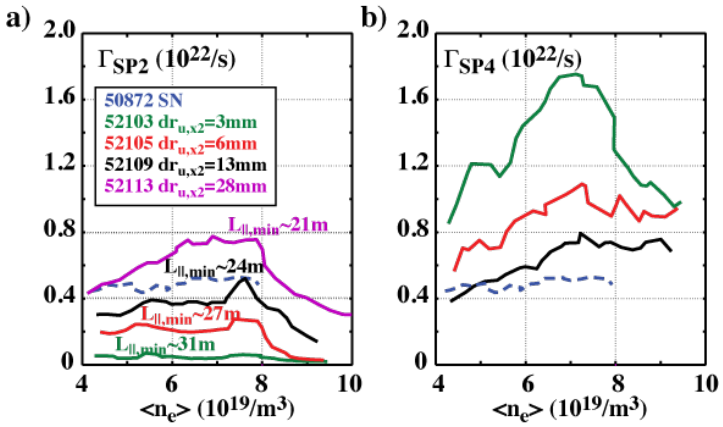

FIG. 7. Density dependence of the ion currents to (a) SP2 and (b) SP4 in LFS SF- configurations with various separations of the x-points.

Motivated by recent EMC3-Eirene predictions of the formation of an impurity radiation zone in the region between the x-points in SF- configurations [22], nitrogen (N_2) was seeded into a SF-, FIG. 8. At sufficiently low plasma density ($\langle n_e \rangle \approx 4\text{x}10^{19}\text{m}^{-3}$), a radiating region indeed develops at the secondary x-point. With continued N_2 seeding this region extends towards the primary x-point, FIG. 8(d). The radiative region does not move with a continuous seeding rate. For the same conditions, a comparable SN configuration displays a strongly radiating region in

front of the inner target that may extend beyond the x-point into the confined plasma, FIG. 8(e). The tendency of the radiating region to remain near an x-point is also seen on the X-divertor and may be a general feature of poloidal flux flaring. A radiative region in the vicinity of the secondary x-point is only obtained for the SF-, if the plasma density is sufficiently low. At higher densities, it also develops a radiating region at the inner strike point, which eventually extends beyond the primary x-point into the core plasma.

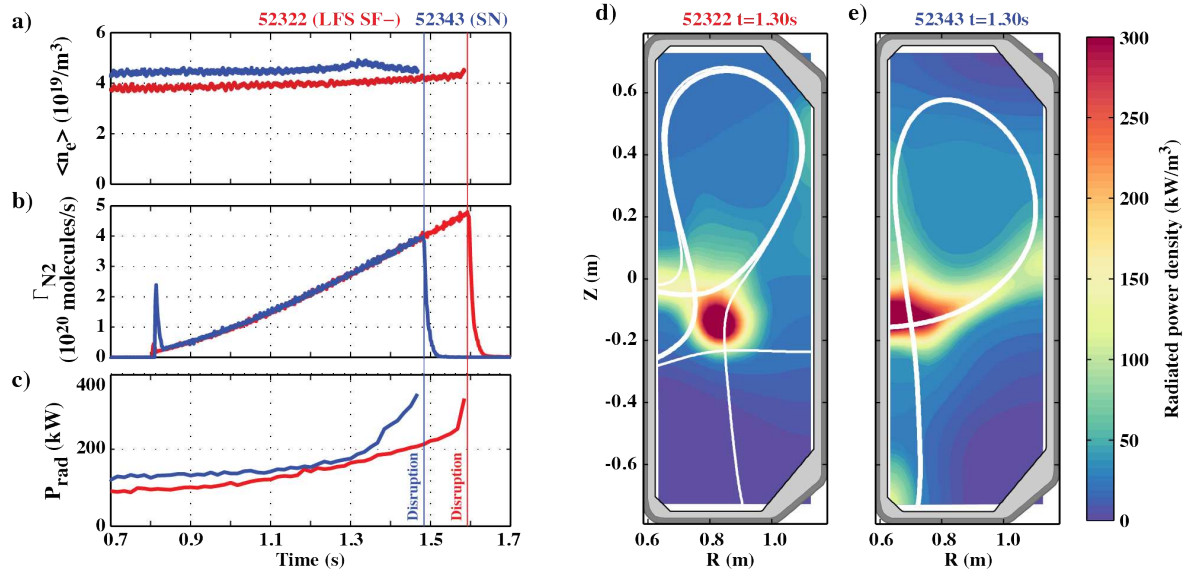

FIG. 8: Evolution of (a) the average density, (b) the N_2 seeding rate and (c) the total radiated power in N_2 seeding experiments in the SF- (red) and SN (blue) configurations and comparison of the radiated power density in (d) the SF- and (e) the SN configurations for the same seeding rate (Γ_{N2}=2.8x10^{20} molecules/s).

4.4. The x-point target divertor

The X-point target divertor [12] is closely related to the SF- configuration. It has the same topology and similar values of $dr_{u,X2}$, but a significantly larger x-point separation. This should also separate the radiation region from the confined plasma limiting detrimental effects on performance. A clear distinction between SF- and x-point target only arises, if the distance between the plasma and the targets is large enough. X-point target configurations have been realised in TCV. Density ramps show no indication of a decreased detachment threshold, despite a 2 to 3-fold connection length increase. This configuration does, however, appear to exert a stabilising effect on radiation location in the vicinity of the secondary x-point [6].

5. Summary

The recent TCV experiments continue previous detachment studies [7] with improved diagnostic coverage and strongly extend the range of geometric variations with an entire suite of alternative magnetic divertor configurations. In Ohmically heated L-mode plasmas, in the standard single-null configuration, the outer divertor leg only detaches at high densities ($n/n_{GW} > 0.5$). The onset of detachment, as indicated by the roll-over of the ion flux to the target, is preceded by a cooling of the divertor leg with the C III cut-off front and ionisation regions moving towards the x-point. The ion flux first decreases in the vicinity of the separatrix before affecting an increasing fraction of the profile. Spectroscopic measurements, however, show that the densities remain highest a few centimetres in front of the target and that the recombination region, unlike in other higher density tokamaks, remains at the target.

Flux expansion and divertor leg length can both vary the connection length, but affect detachment behaviour in different ways. Increasing the flux expansion has only a weak effect the detachment onset, consistent with $n_u(T_t = const.) \propto L_{||}^{-2/7}$ predicted by the extended 2-point model. Conversely, increasing the leg length, which primarily changes $L_{||}$, has a strong facilitating effect on detachment. The difference may be explained by an increase of $\lambda_{q,u}$ observed in low density attached plasmas [14]. A corresponding decrease of $q_{||,0}$ together with $n_u(T_t = const.) \propto q_{||}^{5/7}$ predicted by the extended 2-point model is sufficient to explain the observed decrease of the density at the onset of detachment. The insensitivity of the detachment threshold to flux expansion is also seen in the investigation of the X divertor. While the effect of flux expansion and leg length on the onset density is different, they both allow for a deeper detachment. The flux flaring of the X divertor is, however seen to impede the movement of the cold front away from the target towards the x-point. Surprising results are obtained in the scan of the target radius, a key element of the Super-X divertor concept. While the expected reduction in $q_{||,t}$ is observed, it again does not translate into an earlier detachment. An increased connection length, obtained through a decrease of the poloidal field in the null region of a snowflake minus configuration, again does not lower the detachment density threshold, but allows for deeper detachment.

In addition to density ramps, TCV has performed N_2 seeding experiments to reduce the heat flux and cool the plasma. Nitrogen seeding experiments have, in particular, confirmed predictions of a radiating region between the x-points of a snowflake minus configuration. Its location is stable with the scenario maintained for many energy confinement times. This is similar to x-point radiation scenarios in the single null configuration [26], but with a distance between the radiating region and the core plasma.

TCV's extreme variations of the divertor geometry test and probe our understanding of divertor and scrape off layer physics. This includes key physical and engineering aspects over a wide range of proposed alternative divertor configurations and, thereby, uniquely contributes in the development of a reliable plasma exhaust solution. Next steps will include increasing the power that can be dissipated in the divertor, extending the studies to H-mode scenarios and extending the comparison between experiments and more sophisticated divertor modelling.

Acknowledgements

This work has been carried out within the framework of the EUROfusion Consortium and has received funding from the Euratom research and training programme 2014-2018 under grant agreement No 633053. The views and opinions expressed herein do not necessarily reflect those of the European Commission. This work was supported in part by the Swiss National Science Foundation and the U.S. Department of Energy under Grant No. DE-SC0010529.

References

[1] ZOHM, H., et al., Nucl. Fusion **53** (2013) 073019.
[2] MEYER, H. et al., Nucl. Fusion **57** (2017) 102014.
[3] LIPSCHULTZ, B., LaBOMBARD, B., TERRY, J. L., BOSWELL, C. and HUTCHINSON, I. H., Fusion Sci. Technol. **51** (2007) 369.
[4] STANGEBY, P.C., "The Plasma Boundary of Magnetic Fusion Devices" (Bristol: Institute of Physics Publishing) chapter 5 (2002).
[5] PETRIE, T.W., et al., Nucl. Fusion 53 (2013) 113024.
[6] THEILER, C., et al., Nucl. Fusion **57** (2017) 072008.
[7] PITTS, R., et al., J. Nucl. Mater. **290-293** (2001) 940-946.
[8] REIMERDES, H, et al., J. Nucl. Mater. **463** (2015) 1196.

[9] KOTSCHENREUTHER, M., VALANJU, P., COVELE, B. and MAHAJAN, S., Phys. Plasmas **20** (2013) 102507.
[10] VALANJU, P.M., KOTSCHENREUTHER, M., MAHAJAN, S. and CANIK, J., Phys. Plasmas **16** (2009) 056110.
[11] RYUTOV, D.D, Phys. Plasmas **14** (2007) 064502.
[12] LABOMBARD, B., et al., Bull. Am. Phys. Soc. **58** (2013) 16.
[13] VERHAEGH, K., et al., "Spectroscopic investigations of divertor detachment in TCV", Nucl. Mater. Energy, doi: 10.1016/j.nme.2017.01.004
[14] MAURIZIO, R., et al., "Divertor power load studies for attached L-mode Single-Null plasmas in TCV", submitted to Nucl. Fusion.
[15] BOEDO, J.A., CROCKER, N., CHOUSAL, L., HERNANDEZ, R., CHALFANT, J., KUGEL, H., RONEY, P., WERTENBAKER, J and NSTX Team, Rev. Sci, Instrum. **80** (2009) 123506.
[16] HARRISON, J.R., et al., "Detachment Dynamics on the TCV Tokamak", Nucl. Mater. Energy, doi: 10.1016/j.nme.2016.10.020.
[17] VIANELLO, N., et al., Nucl. Fusion **57** (2017) 116014.
[18] POTZEL, S, WISCHMEIER, M., BERNERT, M., DUX, R., MÜLLER, H.W., SCARABOSIO, A. and the ASDEX Upgrade Team, Nucl. Fusion **54** (2014) 013001.
[19] GALLO, A. et al, "Effect of plasma geometry on divertor heat flux spreading: MONALISA simulations and experimental results from TCV", Nucl. Mater. Energy, doi: 10.1016/j.nme.2016.10.003.
[20] COVELE, B., KOTSCHENREUTHER, M., MAHAJAN, S., VALANJU, P., LEONARD, A., WATKINS, J., MAKOWSKI, M., FENSTERMACHER M. and SI, H., Nucl. Fusion **57** (2017) 086017.
[21] LIPSCHULTZ, B., PARRA, F.I., HUTCHINSON, I.H., Nucl. Fusion **56** (2016) 056007.
[22] LUNT, T., CANAL, G.P., DUVAL, B.P., FENG, Y., LABIT, B., MCCARTHY, P., REIMERDES, H., VIJVERS, W.A.J. and WISCHMEIER, M., Plasma Phys. Control. Fusion **58** (2016) 045027.
[23] RYUTOV, D.D., COHEN, R.H., FARMER, W.A., ROGNLIEN, T.D. and UMANSKY, M.V., Phys. Scr **89** (2014) 088002.
[24] REIMERDES, H., et al., Plasma Phys. Control. Fusion **55** (2013) 124027.
[25] LABIT, B., et al., "Experimental studies of the snowflake divertor in TCV", Nucl. Mater. Energy, doi: 10.1016/j.nme.2017.03.013.
[26] BERNERT, M., et al., "Power exhaust by SOL and pedestal radiation at ASDEX Upgrade and JET", Nucl. Mater. Energy, doi: 10.1016/j.nme.2016.12.029.